Lunar neutrinos

S. Demidov[1,2] and D. Gorbunov[1,2]

[1]*Institute for Nuclear Research of the Russian Academy of Sciences, Moscow 117312, Russia*
[2]*Moscow Institute of Physics and Technology, Dolgoprudny 141700, Russia*

Cosmic rays bombard the lunar surface producing mesons, which attenuate inside the regolith. They get slower and decay weakly into mostly sub-GeV neutrinos leaving the surface. Thus the Moon shines in neutrinos. Here we calculate spectra of low-energy neutrinos, which exhibit bright features potentially recognizable above isotropic neutrino background in the direction towards the Moon. Their observation, though a very challenging task for future neutrino large volume experiments, would make the Moon the nearest astrophysical source for which the concept of multimessenger astronomy truly works. Remarkably, some features of the lunar neutrino flux are sensitive to the surface mass density of the Moon.

I. INTRODUCTION

So far we have observed only a single extra-terrestrial permanent neutrino source, that is the Sun. Neutrinos can emerge upon hadron production in astrophysical sources, see e.g., [1,2]; however, the powerful ones are at quite large distances, so the individual positional identification requires an angular resolution far beyond the capabilities of the operating neutrino telescopes. Naturally, it is tempting to start with a close source with obvious production mechanism to have both theoretical prediction robust and positional identification reliable.

A promising source of this kind is the Moon. Cosmic rays (CR) hit its surface freely provided the absence of atmosphere. They initiate hadronic cascades developing inside the regolith, and numerous mesons weakly decay producing neutrinos. The cosmic ray spectrum degrades with energy and the scattering off regolith slows down the mesons, so the largest neutrino flux is expected from stopped mesons and muons. Hence the Moon becomes a source of neutrinos in sub-GeV energy range to be observed in the sky by neutrino telescopes. Semianalytic calculations of high energy (above 10 GeV) part of the neutrino energy spectrum were performed in the study [3] (see also [4,5] for earlier studies). It showed a suppression of the lunar neutrino flux as compared to the atmospheric one, calculated over the Moon's solid angle, by factor of 10^{-2}–10^{-4} depending on neutrino energy. Remarkably, both lunar and atmospheric neutrinos have the same origin in cosmic rays.

In this paper we calculate the low energy part (from 10 MeV to about 10 GeV) of the lunar neutrino spectrum and compare the lunar neutrino flux at the Earth with the isotropic background from atmospheric and supernova neutrinos. We numerically simulate interactions of cosmic rays with the regolith and count neutrinos produced in meson and muon decays. We observe that although the ratio of total lunar to atmospheric neutrino fluxes in the low energy range is close to unity (contrary to the more energetic part) their spectra are quite different. This observation makes it potentially possible to distinguish between neutrinos of different origin, although the small Moon's solid angle with respect to the whole sky ($\sim 5 \times 10^{-6}$) makes the task of lunar neutrino detection a great challenge, even for near future neutrino experiments at the Earth.

Note that previous studies of the impact of cosmic ray bombarding the Moon include, in particular, simulations of the production of cosmogenic nuclides [6] and gamma-ray albedo [7]. Induced by the cosmic rays, γ-ray emission from the Moon was measured by FERMI [8,9]. A Moon shadow in high-energy cosmic rays was measured in numerous experiments; most recently by ANTARES [10,11] and IceCube [12,13]. Possible implications of interactions of astrophysical neutrinos in the Moon were discussed in [14].

II. SIMULATION DETAILS AND RESULTS

Absence of atmosphere makes the Moon a very effective cosmic ray dump. Namely, dominant source of neutrinos are pions and kaons, which emerge in collisions of cosmic rays with the Moon soil and stop before decay, hence producing monoenergetic neutrinos.
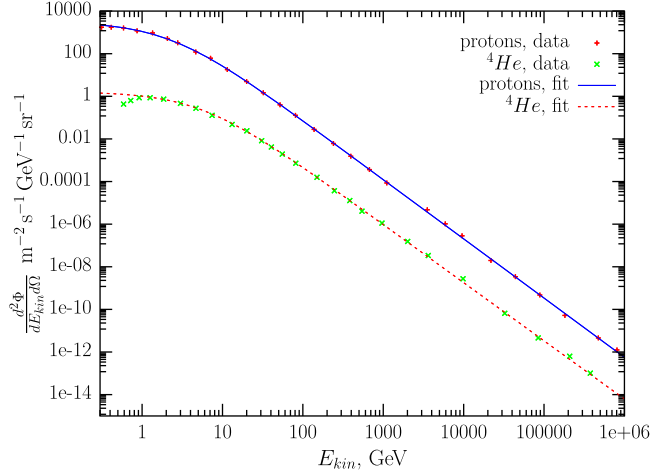
FIG. 1.   Proton and ^{4}He measured fluxes (the latter is scaled by a factor of 10^{-2} as in PDG) and numerical fits (1) and (2) used in our analysis.

To simulate neutrino flux from the Moon we exploit GEANT toolkit [15]. We involve the cosmic ray spectra dominated by protons and ^{4}He components. We fit the corresponding plot from particle data group (PDG) [16] by a power-law function (see Fig. 1). The fits can be described as (units are $m^{-2}\,s^{-1}\,sr^{-1}\,GeV^{-1}$)

$$\frac{d^2\Phi}{dE_{kin}d\Omega} = \frac{2.7 \times 10^4}{(E_{kin} + 2.3 m_p)^{2.78}} \quad \text{for protons,} \quad (1)$$

$$\frac{d^2\Phi}{dE_{kin}d\Omega} = \frac{1.5 \times 10^4}{(E_{kin} + 1.4 m_{He})^{2.73}} \quad \text{for } ^4\text{He,} \quad (2)$$

TABLE I.   Chemical composition of lunar soil, adopted from Ref. [17].

Element	Composition (wt%)
SiO_2	45.5
Al_2O_3	19.5
CaO	13.8
FeO	10.0
MgO	8.3
TiO_2	2.3
Na_2O	0.6

where E_{kin} is the kinetic energy of the nuclei, and m_p and m_{He} are masses of proton and ^{4}He nuclei respectively. In simulations we set the threshold kinetic energy E_{kin}^{th} to 0.4 GeV for protons and to 0.8 GeV for ^{4}He. We checked that cosmic rays of lower energies produce rather small amounts of neutrinos.

The Moon chemical composition is taken as shown in Table I which is the average of chemical compositions of *Maria* and *Highlands* parts of the Moon surface (see e.g., [17]). For the lunar soil density we take $\rho \approx 1.5$ g/cm^3 which corresponds to an average density of the upper layer of regolith. We assume the isotropic arrival directions of the cosmic rays. We track the secondary particles produced by the collisions of cosmic rays with the lunar surface using GEANT (we exploit the FTFP-BERT physics model). Within the simulation we count all electron and muon neutrinos, and antineutrinos leaving the Moon. Neutrino energy allows for constructing spectra. The fluxes of τ-neutrinos and antineutrinos at production are negligible as compared to those which emerge due to oscillations, which we discuss below.
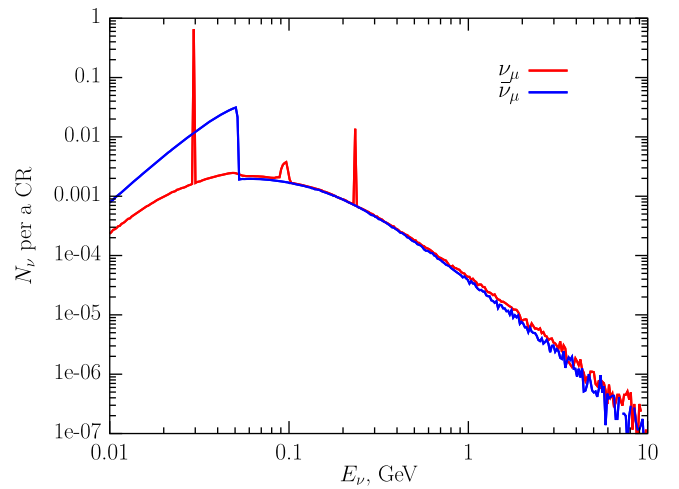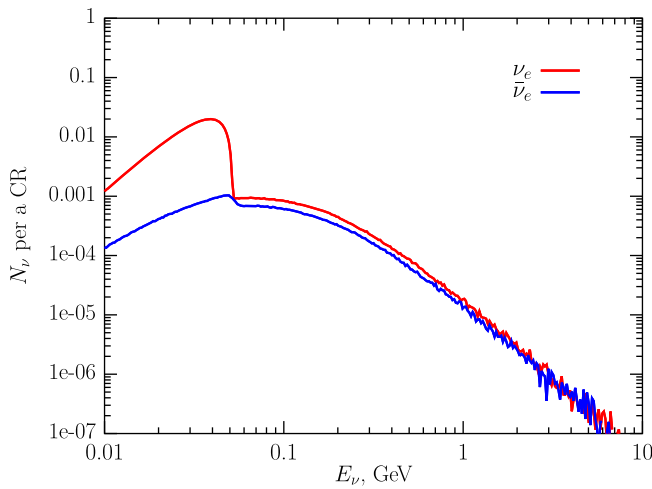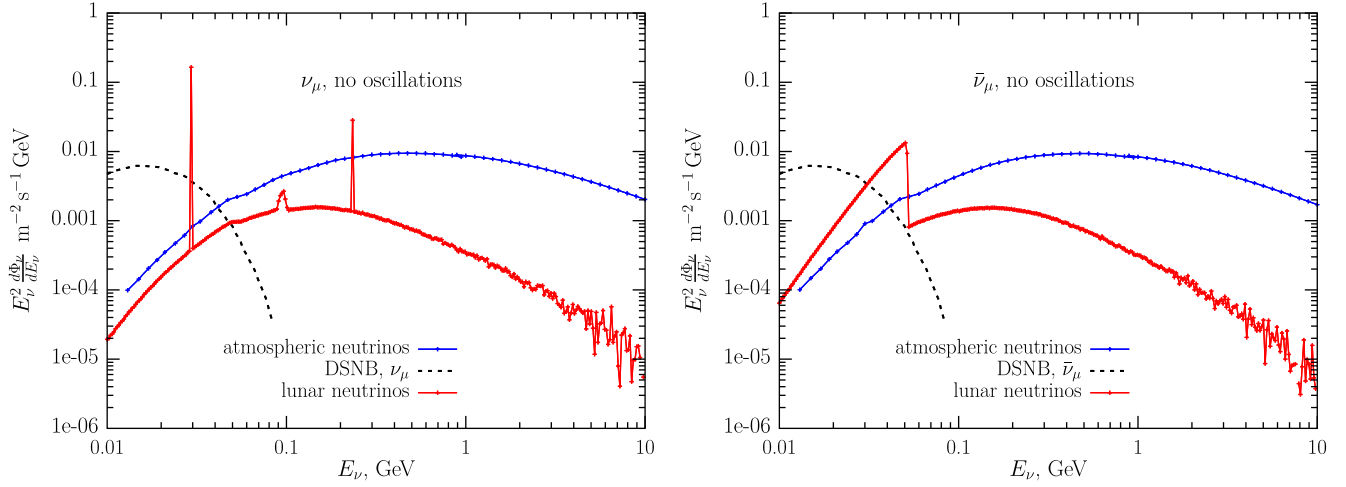

FIG. 2.   Spectra of electron (left panel) and muon (right panel) neutrinos and antineutrinos normalized to a single CR. The energy goes from 10 MeV to 10 GeV in the decimal logarithmic scale with 320 bins.

FIG. 3. Fluxes of lunar neutrinos ν_μ and antineutrinos $\bar{\nu}_\mu$ (red lines) in comparison with atmospheric (blue) and diffuse supernova (dashed black) neutrino fluxes calculated within a fraction of solid angle $\frac{\pi R_{\text{Moon}}^2}{4\pi L_{\text{Moon}}^2}$. No oscillations are taken into account.

FIG. 4. Fluxes of lunar neutrinos ν_e and antineutrinos $\bar{\nu}_e$ (red lines) in comparison with atmospheric (blue) and diffuse supernova (dashed black) neutrino fluxes calculated within a fraction of solid angle $\frac{\pi R_{\text{Moon}}^2}{4\pi L_{\text{Moon}}^2}$. No oscillations are taken into account.
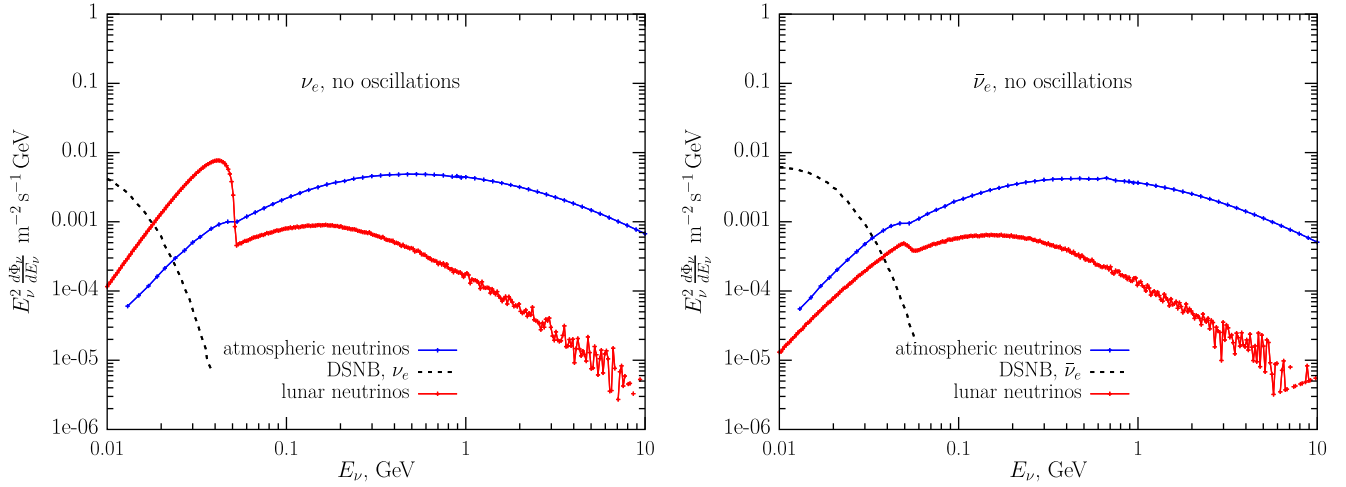
In Fig. 2 we show the obtained spectra of electron (left panel) and muon (right panel) neutrinos and antineutrinos $N_\nu(E_\nu)$ normalized to a single cosmic ray hitting the Moon; we simulated about 1.5×10^7 CR events and the resulting neutrino events are distributed over 320 uniform logarithmic energy bins. No oscillations are taken into account at this stage. Most of the neutrinos come from charged pion and kaon decays as well as from decays of secondary muons. Initially, pions π^+ and π^- are produced in close fractions. They lose their energies in the course of elastic collisions with nuclei, interact and stop in the lunar soil.

Most parts of π^- get captured by nuclei via Coulomb attraction [18] and do not produce neutrinos within the discussed energy interval 10 MeV–10 GeV. On the other hand, stopped π^+ produce a monochromatic line of ν_μ at energy $E_\nu \approx 29.8$ MeV and antimuons μ^+ which also stop in media and undergo the decay $\mu^+ \rightarrow e^+ \nu_e \bar{\nu}_\mu$, yielding neutrinos of energies below the threshold at $E_\nu \approx 52.8$ MeV. A similar picture is valid for charged kaons, which produce a monochromatic ν_μ line at $E_\nu \approx 235.6$ MeV. On the right panel of Fig. 2 two peaks at $E_\nu \sim 30$ MeV and 236 MeV in the red histogram
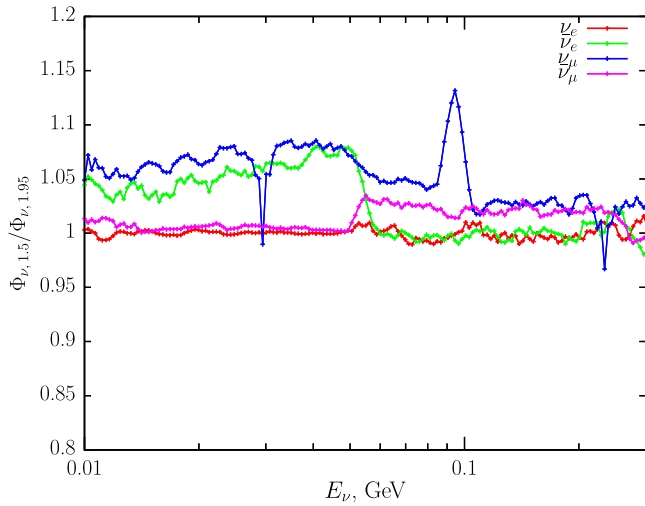
FIG. 5. Ratio of lunar neutrino flux at production calculated for different regolith densities, 1.5 g/cm³ and 1.95 g/cm³, respectively.

correspond to those monochromatic neutrinos. The widths of 30 MeV and 236 MeV lines on this plot are chosen to be equal to the bin width. Their actual widths are considerably narrower, and hence the actual heights are considerably higher. We clarify their contribution numerically in due course. There is also a small bump at energies somewhat below the muon mass, $E_\nu \approx$ 100 MeV. It appears from the process of muon capture by nuclei with subsequent conversion to neutrinos, i.e., $\mu^- + p \to n + \nu_\mu$, see e.g., [19]. The spectra of $\bar{\nu}_\mu$ and ν_e at $E_\nu \lesssim 53$ MeV correspond to neutrinos from decays of antimuons μ^+, most of which decay at rest. We note in passing that neutrinos from stopped pions and kaons were studied previously in different contexts (and in particular in searches for a signal from dark matter annihilations in the Sun) in Refs. [20–24].

Now we turn to the calculation of lunar neutrino flux at the Earth. The lunar regolith emits neutrinos in all
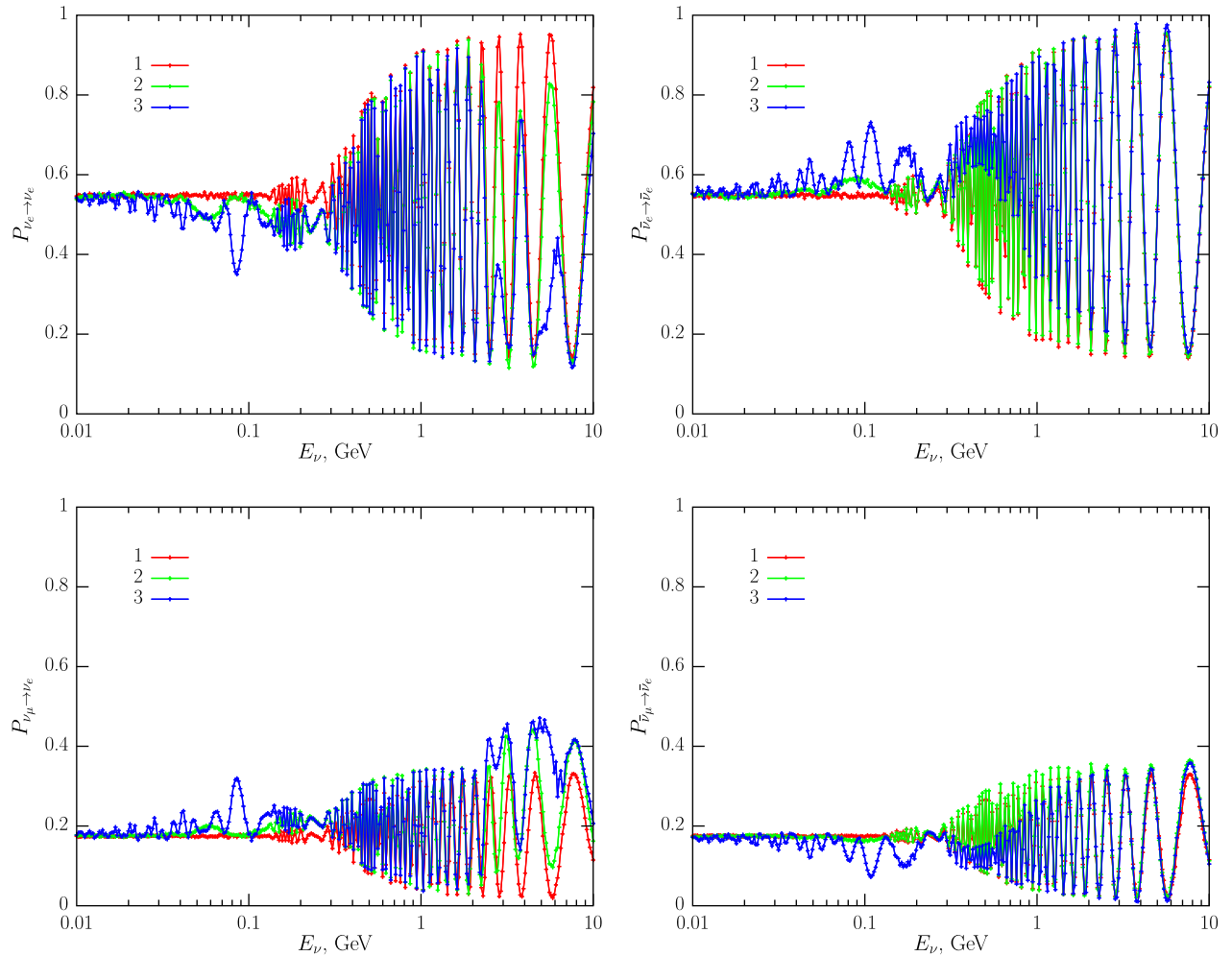
FIG. 6. Oscillation probabilities of lunar neutrinos at the Earth, $P_{\nu_e \to \nu_e}$ (upper left), $P_{\bar{\nu}_e \to \bar{\nu}_e}$ (upper right), $P_{\nu_\mu \to \nu_e}$ (lower left), $P_{\bar{\nu}_\mu \to \bar{\nu}_e}$ (lower right). Different curves correspond to probabilities calculated 1) without matter effects; 2) with matter effects in the Moon only; 3) with matter effects in the Moon and the Earth. See main text for details.
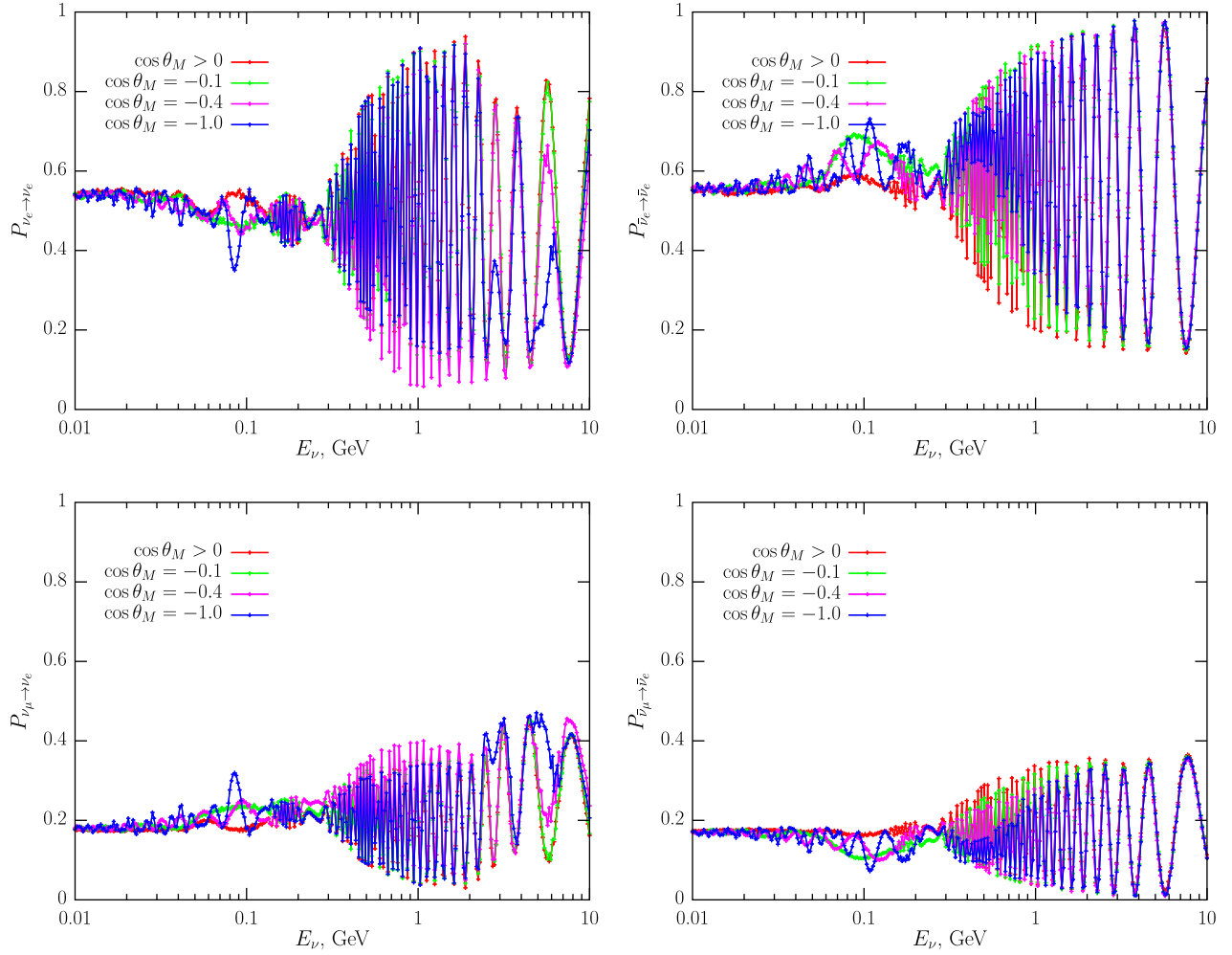
FIG. 7. Oscillation probabilities to electron (anti)neutrinos at the Earth for different zenith angles of the Moon.

directions.[1] Using total isotropic flux Φ_{CR} of cosmic rays integrated over energy we can find the number of cosmic ray particles bombarding the Moon per second

$$\int 2\pi d(\cos\theta)\cos\theta dS\Phi_{CR} = \pi \cdot 4\pi R^2_{Moon}\Phi_{CR}, \quad (3)$$

where R_{Moon} is the Moon radius. Then, the neutrino ν_α flux at the Earth can be written as

$$\Phi_{\nu_\alpha} = \frac{1}{4\pi L^2_{Moon}} \times \pi \cdot 4\pi R^2_{Moon}\Phi_{CR}N_{\nu_\alpha}(E_\nu)$$

$$\equiv \pi\left(\frac{R_{Moon}}{L_{Moon}}\right)^2 \Phi_{CR}N_{\nu_\alpha}(E_\nu), \quad (4)$$

where L_{Moon} is the average distance from the Earth to the Moon. Let us note that given the Moon's orbit perigee of about 362600 km and apogee of about 405400 km one

expects monthly variations of the amplitude of lunar neutrino flux Φ_{ν_α} of about 12%.

In Figs. 3 and 4 we present differential neutrino fluxes multiplied by energy squared, i.e., $E^2_\nu \frac{d\Phi_\nu}{dE_\nu}$ (in units of m^{-2} s^{-1} GeV), for muon and electron (anti)neutrinos (red lines) in comparison with atmospheric neutrino flux (blue lines) taken from [25,26] and diffuse supernova neutrino background (DSNB) flux (dashed black lines) taken from [27] in the direction towards the Moon, which are obtained[2] by multiplying the overall neutrino fluxes (no oscillations) by a factor equal to the fraction of the celestial sphere occupied by the Moon, $\frac{\Delta\Omega}{4\pi} = \frac{\pi R^2_{Moon}}{4\pi L^2_{Moon}} \approx 5 \times 10^{-6}$. Comparing, for instance, lunar and atmospheric neutrinos in the energy interval from 10 MeV to 1 GeV we find that ratio of their energy integrated fluxes within the same solid angle is close to unity (about 1.4–1.5). At the same time, the

---

[1] Neglecting small cosmic ray shadow by the Earth at the Moon.

[2] Let us note that that atmospheric neutrino flux depends on the positioning of the detector; the difference is within a factor of two [25].
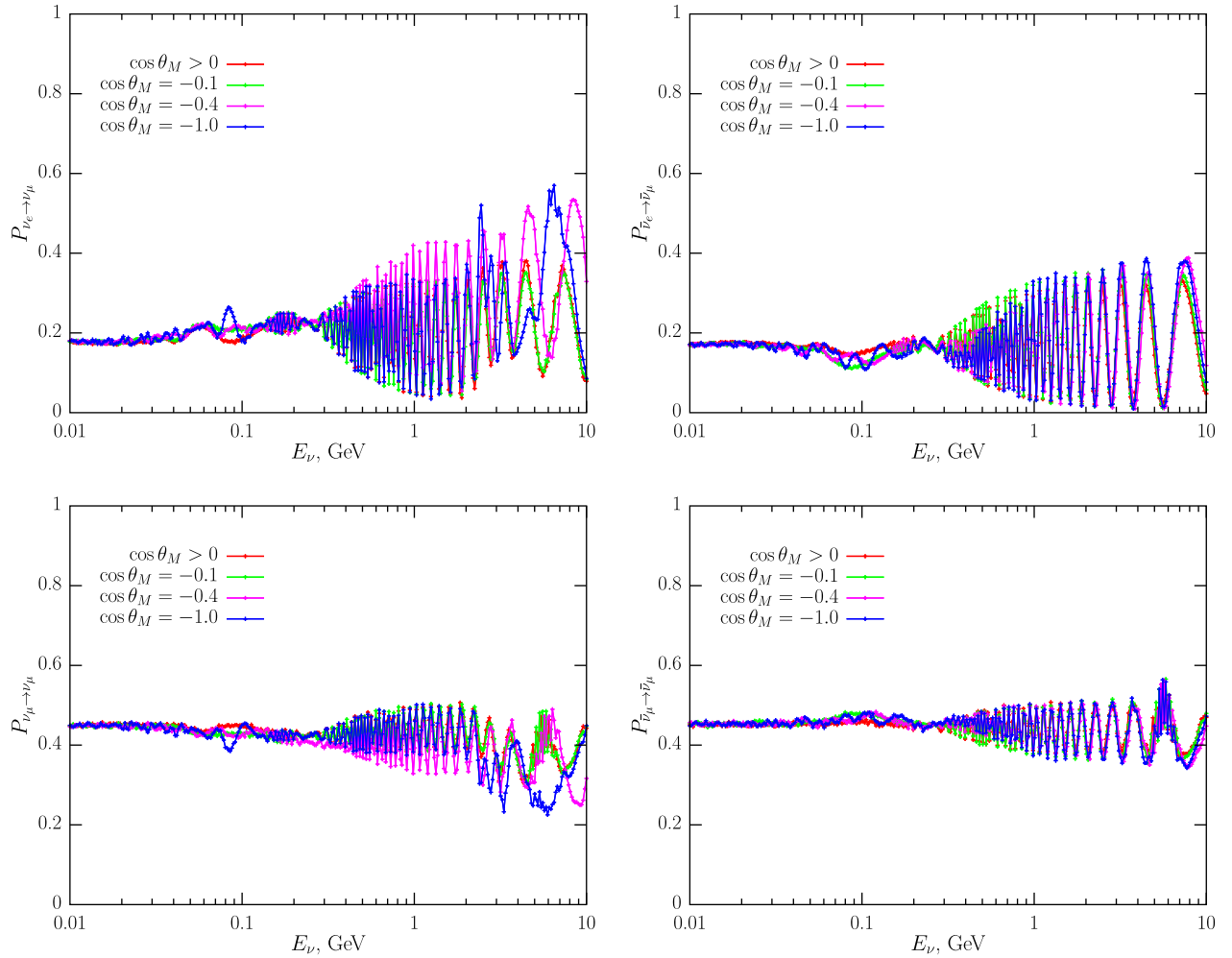
FIG. 8. Oscillation probabilities for muon (anti)neutrinos at the Earth for different zenith angles of the Moon.

shapes of their energy spectra are drastically different due to prominent features related to peculiarities of neutrino production in the Moon. In particular, for an idealized neutrino detector having an energy resolution of 10% the fluxes of ν_μ from the Moon are about 0.14 m^{-2} s^{-1} and 0.0033 m^{-2} s^{-1} for neutrino energies 29.8 MeV and 236 MeV, respectively, to be compared with atmospheric ν_μ neutrino fluxes 0.0028 m^{-2} s^{-1} and 0.0034 m^{-2} s^{-1}, calculated over the solid angle of the Moon (without oscillations).

As we discussed above, interactions of parent mesons and muons in the media have a great impact on the spectra of neutrinos produced in collisions of cosmic rays with the Moon's surface. To illustrate this point we perform the same numerical simulation taking somewhat larger values of the regolith density, $\rho = 1.95$ g/cm^3. In Fig. 5 we show the ratios of neutrino fluxes with densities 1.5 g/cm^3 and 1.95 g/cm^3, respectively, for all neutrino flavors at production. We see the change of density has the most prominent impact on ν_μ flux. In particular, in the lower-

density matter the flux of ν_μ is higher than the peaks at 29.7 MeV and 236 MeV. This corresponds to an increase in probability for mesons π^+ and K^+ (and subsequent μ^+) to decay in flight. At the same time, ν_μ flux at the resonant energies, corresponding to decay of mesons at rest, decreases. We also observe an increase of ν_μ flux at the region around 100 MeV where these neutrinos appear from $\mu^- - \nu_\mu$ conversion on nuclei. Fluxes of $\bar{\nu}_e$ are also higher at energies corresponding to neutrino production from stopped muons μ^-. This is related to a lower probability for π^- to be captured by nuclei in less dense media. At the same time fluxes of ν_e and $\bar{\nu}_\mu$, which come from decays of μ^+, in this energy range are almost unchanged. Note that we omit the part of the plot at larger energies where small statistics do not allow us to clearly see the density impact. It is worth noting that most neutrinos in the interesting energy range are produced in the surface upper layer of $\lesssim 1$ m depth. One can also expect dependence of lunar neutrino flux on the density as well as on the composition of the
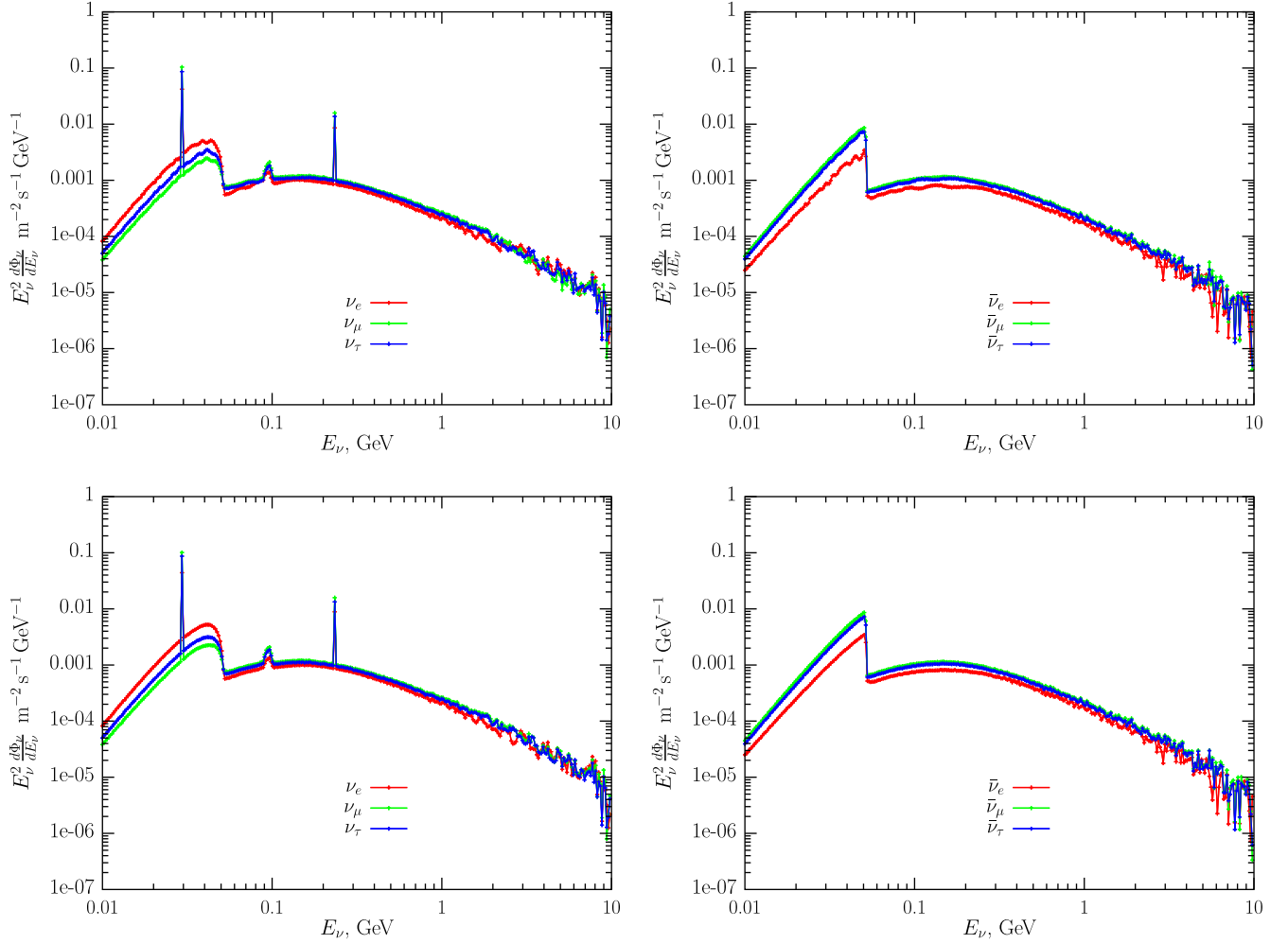
FIG. 9. Fluxes of lunar neutrinos (left) and antineutrinos (right) calculated accounting for neutrino oscillations for $\cos\theta_M > 0$ (upper panels) and after averaging over position of the Moon in the sky (lower panels).

regolith. Hence, the measurement of the neutrino spectra provides us with a tool to investigate the lunar surface density.

Now let us study impact of neutrino oscillations on lunar neutrinos. As most of them are produced in the surface region of the Moon, the corresponding neutrino oscillation probabilities should be averaged over the production point. The oscillation lengths for neutrinos of 10 MeV– 1 GeV is considerably smaller than the baseline (which is about L_{Moon}) and for the lower part of this energy range is even smaller than the radius of the Moon. This results in almost incoherent neutrino flavor transitions for the softest part of lunar neutrino spectra. However, matter effects in the Moon and the Earth may be important.[3] To model neutrino oscillation in the Moon we use the profile of lunar density from Ref. [28] and we adopt the PREM model [29] for the Earth structure to describe neutrino oscillations on the

Earth. We numerically solve the Schrödinger equation for the neutrino wave function. For the Pontecorvo-Maki-Nakagawa-Sakata (PMNS) matrix elements we take the best fit to neutrino oscillation experiments from Ref. [30] for normal neutrino mass hierarchy as an example. First, to demonstrate the impact of the neutrino oscillation in matter of the Moon and the Earth we show in Fig. 6 neutrino oscillation probabilities $P_{\nu_e\to\nu_e}$ (upper left), $P_{\bar{\nu}_e\to\bar{\nu}_e}$ (upper right), $P_{\nu_\mu\to\nu_e}$ (lower left), $P_{\bar{\nu}_\mu\to\bar{\nu}_e}$ (lower right) for three different cases: 1) no matter effects in the Moon and the Earth; 2) with matter effects in the Moon only; 3) matter effects in the Moon and the Earth. In the latter case we consider neutrino propagating through the center of the Earth, which implies that we account for the neutrino signal only when the Moon is in Nadir in a real experiment. In all three cases we average over the production point on the Moon surface and took $L_{\text{Moon}} = 384000$ km as the distance between the Earth and the Moon. We checked that variation of L_{Moon} due to ellipticity of the Moon orbit results only in minor corrections to the oscillation

---

[3]We are grateful to an anonymous referee for raising this question.

probabilities. Also, we average over neutrino energy inside each of 320 energy bins. Second, in Fig. 7 we show dependence of oscillation probabilities for electron (anti) neutrinos on zenith angle θ_M of the Moon (the case $\cos\theta_M > 0$ corresponds to the Moon above the horizon; hence no matter effects in the Earth). In Fig. 8 we show the same probabilities but for muon (anti)neutrinos.

Impacts from matter effect in the Moon and the Earth results in deviations from averaged neutrino oscillation probabilities and are clearly visible in those figures. However, (see Sec. III) to make these studies feasible, one needs to collect a sufficient amount of lunar neutrinos from each position of the Moon, which implies an unrealistically large operation time for the experiment. In this case one may sum lunar neutrinos along the Moon trajectories, which average the matter effect in the Earth, but keep intact the matter effect in the Moon. In Fig. 9 we show resulting spectra of lunar neutrinos and antineutrinos at the Earth calculated for two cases: 1) assuming the Moon to be above the horizon, which implies no matter effect in the Earth, and 2) averaging over the position of the Moon on the full sky. In a realistic experimental setup additional averaging of oscillations comes from finite energy and directional resolution. A detailed study of this question is beyond the scope of this paper and generically depends on the experimental parameters. We will comment on that in the next section. However, from the plots of Fig. 9 one concludes that though the difference is recognizable by eye, in a realistic experiment the matter effect in the Earth has no observable effect at all.

Let us note in passing that although here we study the oscillations numerically, one can use an analytical approach to describe the evolution of low energy neutrinos (see e.g., [31,32]). Matter effects of neutrino propagation in the Moon may be potentially used to obtain information about its inner structure similar to the studies for the Earth (see e.g., Refs. [33–35]).

III. DISCUSSION AND CONCLUSIONS

In this paper we calculated the flux of neutrinos originating from cosmic rays hitting the Moon's surface. Apposed to the earlier study [3] we concentrated on the low energy ($\lesssim 10$ GeV) part of the neutrino energy spectrum. Although lunar neutrinos have the same origin as atmospheric ones, the absence of atmosphere at the Moon makes the spectrum of the former to be quite peculiar and sensitive to the mass density of the surface layer. In particular, it appears to be shifted to lower energies where neutrinos originate from decays of mesons stopped in the regolith. Without neutrino oscillations the very low energy part (less than about 52.8 MeV) of the lunar neutrino spectrum at the Earth exceeds the atmospheric neutrino flux from the Moon's solid angle by up to an order of magnitude for

ν_e and $\bar\nu_\mu$, while the spectrum of ν_μ exhibits two narrow peaks at energies $E_\nu \approx 29.8$ MeV and 235.6 MeV corresponding to neutrinos from π^+ and K^+ decays. Oscillations of neutrinos mix those effects between all neutrino flavors. At energies lower than about 20 MeV–50 MeV the lunar neutrino flux is comparable with that of DSNB within the Moon's solid angle. Contrary to atmospheric and diffuse neutrinos, the lunar neutrino flux is expected to endue a periodic dependence with amplitude of about 12% from small ellipticity of the Moon's orbit. These peculiarities, including explicit binding to the direction of the Moon, can be used to search for lunar neutrinos in future neutrino experiments and to distinguish them from atmospheric neutrino and diffuse supernova neutrino background.

At present, neutrino detectors used or planned for study of sub-GeV neutrinos include water Cerenkov (WC) detectors such as Hyper-Kamiokande [36,37] and its predecessor Super-Kamiokande, liquid scintillator (LS), and liquid argon time projection chambers (LArTPC). The latter representative examples are JUNO [38] and DUNE [39], respectively. WC detectors can be more easily realized in a large volume which is a crucial requirement for the detection of the pretty low neutrino flux from the Moon. However, the neutrino-nucleon scattering correlation between the direction of charged lepton and incoming neutrino is weak for neutrinos from sub-GeV energy range. Moreover, for such neutrino energies an additional background in WC detectors comes from invisible muons. LS and LArTPC detectors are free from this type of background. Still, typical detection channels used in LS detectors do not provide very much information about neutrino direction in the considered energy range. LArTPC detectors on the other hand, can provide not only energy information but also a directional information (see e.g., [24]) as for them it is possible to reconstruct positions of charged leptons and nucleons [40]. Still, even if very large exposures can be realized here, an angular resolution of these detectors is still quite poor at present as compared to the angular size of the Moon on the sky. We conclude that the detection of lunar neutrinos would require not just large but huge neutrino detectors with exceptional energy and strong angular resolution—a task which may one day be feasible.

[1] L. A. Anchordoqui *et al.*, Cosmic neutrino pevatrons: A brand new pathway to astronomy, astrophysics, and particle physics, JHEAp **1–2,** 1 (2014).

[2] E. Vitagliano, I. Tamborra, and G. Raffelt, Grand unified neutrino spectrum at earth: Sources and spectral components, Rev. Mod. Phys. **92,** 045006 (2020).

[3] R. Miller and T. Cohen, Cosmic-ray induced neutrino fluxes at the Moon: A semi-analytic approach, Astropart. Phys. **25,** 368 (2006).

[4] L. V. Volkova and G. T. Zatsepin, The energy spectra of muons and neutrinos generated by cosmic rays in different substances., in *International Cosmic Ray Conference*, Vol. 1 of International Cosmic Ray Conference (The Institute of Physics and The Physical Society, London, 1965), p. 1039.

[5] L. V. Volkova, *Fluxes of Muons and Neutrinos Generated by Primary Radiation on the Moon* (Springer Netherlands, Dordrecht, 1989), pp. 141–144.

[6] Y. Li, X. Zhang, W. Dong, Z. Ren, T. Dong, and A. Xu, Simulation of the production rates of cosmogenic nuclides on the moon based on geant4, J. Geophys. Res. **122,** 1473 (2017).

[7] I. V. Moskalenko and T. A. Porter, The gamma-ray albedo of the moon, Astrophys. J. **670,** 1467 (2007).

[8] A. Abdo *et al.*, FERMI observations of γ-ray emission from the Moon, Astrophys. J. **758,** 140 (2012).

[9] M. Ackermann *et al.* (Fermi-LAT Collaboration), Measurement of the high-energy gamma-ray emission from the Moon with the Fermi Large Area Telescope, Phys. Rev. D **93,** 082001 (2016).

[10] C. Distefano (ANTARES Collaboration), On the detection of the Moon shadow with the ANTARES neutrino telescope, Nucl. Instrum. Methods Phys. Res., Sect. A **626–627,** S223 (2011).

[11] A. Albert *et al.* (ANTARES Collaboration), The cosmic ray shadow of the Moon observed with the ANTARES neutrino telescope, Eur. Phys. J. C **78,** 1006 (2018).

[12] D. Boersma, L. Gladstone, and A. Karle (IceCube Collaboration), Moon shadow observation by IceCube, arXiv:1002.4900.

[13] M. Aartsen *et al.* (IceCube Collaboration), Observation of the cosmic-ray shadow of the Moon with IceCube, Phys. Rev. D **89,** 102004 (2014).

[14] D. Fargion, P. Oliva, P. G. de Sanctis Lucentini, and M. Y. Khlopov, Signals of HE atmospheric μ decay in flight around the Sun's albedo versus astrophysical ν_μ and ν_τ traces in the Moon shadow, Int. J. Mod. Phys. D **27,** 1841002 (2018).

[15] S. Agostinelli *et al.* (GEANT4 Collaboration), GEANT4–a simulation toolkit, Nucl. Instrum. Methods Phys. Res., Sect. A **506,** 250 (2003).

[16] M. Tanabashi *et al.* (Particle Data Group Collaboration), Review of particle physics, Phys. Rev. D **98,** 030001 (2018).

[17] S. R. Taylor, *Lunar Science: A Post-Apollo View; Scientific Results and Insights from the Lunar Samples* (Pergamon Press, New York, 1975).

[18] L. Ponomarev, Molecular structure effects on atomic and nuclear capture of mesons, Annu. Rev. Nucl. Part. Sci. **23,** 395 (1973).

[19] D. Measday, The nuclear physics of muon capture, Phys. Rep. **354,** 243 (2001).

[20] J. Spitz, Cross section measurements with monoenergetic muon neutrinos, Phys. Rev. D **89,** 073007 (2014).

[21] C. Rott, J. Siegal-Gaskins, and J. F. Beacom, New sensitivity to solar WIMP annihilation using low-energy neutrinos, Phys. Rev. D **88,** 055005 (2013).

[22] N. Bernal, J. Martin-Albo, and S. Palomares-Ruiz, A novel way of constraining WIMPs annihilations in the Sun: MeV neutrinos, J. Cosmol. Astropart. Phys. 08 (2013) 011.

[23] C. Rott, S. In, J. Kumar, and D. Yaylali, Dark matter searches for monoenergetic neutrinos arising from stopped meson decay in the sun, J. Cosmol. Astropart. Phys. 11 (2015) 039.

[24] C. Rott, S. In, J. Kumar, and D. Yaylali, Directional searches at DUNE for Sub-GeV monoenergetic neutrinos arising from dark matter annihilation in the sun, J. Cosmol. Astropart. Phys. 01 (2017) 016.

[25] G. Battistoni, A. Ferrari, T. Montaruli, and P. Sala, The atmospheric neutrino flux below 100-MeV: The FLUKA results, Astropart. Phys. **23,** 526 (2005).

[26] M. Honda, M. Sajjad Athar, T. Kajita, K. Kasahara, and S. Midorikawa, Atmospheric neutrino flux calculation using the NRLMSISE-00 atmospheric model, Phys. Rev. D **92,** 023004 (2015).

[27] C. A. J. O'Hare, A. M. Green, J. Billard, E. Figueroa-Feliciano, and L. E. Strigari, Readout strategies for directional dark matter detection beyond the neutrino background, Phys. Rev. D **92,** 063518 (2015).

[28] J. G. Williams, A. S. Konopliv, D. H. Boggs, R. S. Park, D.-N. Yuan, F. G. Lemoine *et al.*, Lunar interior properties from the grail mission, J. Geophys. Res. **119,** 1546 (2014).

[29] A. M. Dziewonski and D. L. Anderson, Preliminary reference earth model, Phys. Earth Planet. Inter. **25,** 297 (1981).

[30] I. Esteban, M. Gonzalez-Garcia, A. Hernandez-Cabezudo, M. Maltoni, and T. Schwetz, Global analysis of three-flavour neutrino oscillations: Synergies and tensions in the determination of θ_{23}, δ_{CP}, and the mass ordering, J. High Energy Phys. 01 (2019) 106.

[31] A. N. Ioannisian, N. A. Kazarian, A. Y. Smirnov, and D. Wyler, A precise analytical description of the earth matter effect on oscillations of low energy neutrinos, Phys. Rev. D **71,** 033006 (2005).

[32] O. L. G. Peres and A. Y. Smirnov, Oscillations of very low energy atmospheric neutrinos, Phys. Rev. D **79,** 113002 (2009).

[33] W. Winter, Atmospheric neutrino oscillations for earth tomography, Nucl. Phys. **B908,** 250 (2016).

[34] A. Ioannisian, A. Smirnov, and D. Wyler, Scanning the Earth with solar neutrinos and DUNE, Phys. Rev. D **96,** 036005 (2017).

[35] P. Bakhti and A. Y. Smirnov, Oscillation tomography of the Earth with solar neutrinos and future experiments, Phys. Rev. D **101,** 123031 (2020).

[36] K. Abe *et al.*, Letter of intent: The hyper-kamiokande experiment—detector design and physics potential, arXiv:1109.3262.

[37] K. Abe *et al.* (Hyper-Kamiokande Proto- Collaboration), Physics potential of a long-baseline neutrino oscillation experiment using a J-PARC neutrino beam and Hyper-Kamiokande, Prog. Theor. Exp. Phys. **2015,** 053C02 (2015).

[38] F. An *et al.* (JUNO Collaboration), Neutrino physics with JUNO, J. Phys. G **43,** 030401 (2016).

[39] R. Acciarri *et al.* (DUNE Collaboration), Long-baseline neutrino facility (LBNF) and deep underground neutrino experiment (DUNE): Conceptual design report, volume 2: The physics program for DUNE at LBNF, arXiv:1512.06148.

[40] C. Anderson *et al.*, The ArgoNeuT Detector in the NuMI Low-Energy beam line at Fermilab, J. Instrum. **7,** P10019 (2012).